Institute of Space and Aeronautical Science, University of Tokyo
Report No. 458, December 1970

Laboratory Experiment on the Solar Wind Interaction with Planetary Bodies

By

Haruya KUBO, Tomizo ITOH and Akira YAMORI

Summary: The electric field generated by the interaction of solar wind with planetary bodies is discussed by the laboratory simulation. It is inferred from this experiment that an upper limit of the electric field behind Moon would be in the order of 10^{-2} V/m, and almost zero behind Venus. The mechanisms generating the electric and the magnetic field by the solar wind interaction are also discussed, and they would respectively be due to charge separation and pressure gradient drift.

1. INTRODUCTION

This model experiment on plasma flow past a body was intended to shed some light on the solar wind interaction with planetary bodies.

Explorer 35 measured magnetic field around the moon, and the electromagnetic properties of the moon was discussed [*1*] [*2*] [*3*]. The model experiment concerning the magnetic field around the moon was performed by Kristoferson [*4*], and the magnetic field configuration similar to that measured by Explorer 35 was obtained.

Explorer 35 also measured the particle shadowing effects by the moon, and the upper limit of the magnetotail electric field was estimated to be 5×10^{-4} V/m [*5*]. Anderson [*6*] introduced a more sensitive method to determine sense and magnitude of the electric field in the magnetotail from the lunar particle shadow.

In this report attention is paid mainly to the electric field behind the planetary bodies downstream of the solar wind. The result of the magnetic field measurement is also reported.

2. EXPERIMENTAL PROCEDURE

Experimental layout is shown in Fig. 1. The solar wind is simulated by a hydrogen plasma stream from a coaxial plasma gun placed about 1.5 m away from the interaction region. The plasma is shot along a magnetic field which has a magnitude of 95 gauss in the interaction region.

The typical properties of the plasma stream in the interaction region, where the model planet is placed are as follows: duration is about 60 μsec; electron

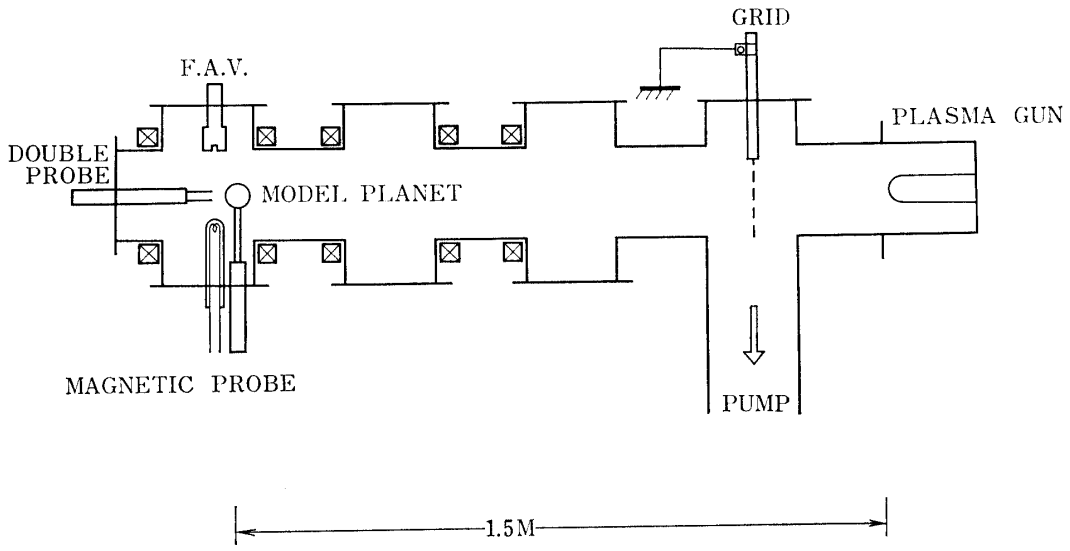

FIG. 1. Experimental layout.

temperature is 8 eV; plasma density is $10^{13}/cm^3$; flow velocity is 5×10^6 cm/sec; plasma diameter is about 8 cm.

A sphere of aluminum and that of an insulator whose diameter is 4 cm, and an air cloud column of 3.5 cm in diameter were used as the model planets. In order to make a gas cloud, a fast acting gas valve was used [7], and a column-shaped gas cloud was formed perpendicularly to the plasma stream for several hundred microseconds. The radius of the gas column expands gradually. The gas density at the center of column is about 10^{16} particles/cm^3 when the plasma stream impinges on it. The gas density distribution was measured by the use of fast ionization gauge in the previous paper[8] and the diameter of the gas column was about 4 cm, but in this work the diameter of the gas cloud was determined to be 3.5 cm by the photograph, as the gas cloud emitted light when the plasma stream impinged on it. This gas cloud can be thought to be staitonary since the interaction time is an order of magnitude smaller than the gas expansion time. These model planets do not simulate the planets with a dynamo-generated magnetic field such as Earth and Jupiter.

The diagnostic tools were a floating double probe for density, temperature and electric field measurements and a magnetic probe for the measurement of a time-dependent magnetic field parallel to the plasma stream ($\tilde{B}_z(r)$).

Fig. 2 shows the method of electric field measurement. The resistance R must be large compared to the plasma impedance of probe spacings, and the product of R and the capacitance C must be small compared to the characteristic time of the electric field variation. For $R=1M\Omega$ and $R=5k\Omega$ almost the same signal levels were obtained. Since the detail of the electric field was seen only in the case of $R=5k\Omega$, we chose $R=5k\Omega$. This floating double probe signal gives the potential difference between probe spacings. $E_r(r)$ was obtained by moving the probe in r-direction.

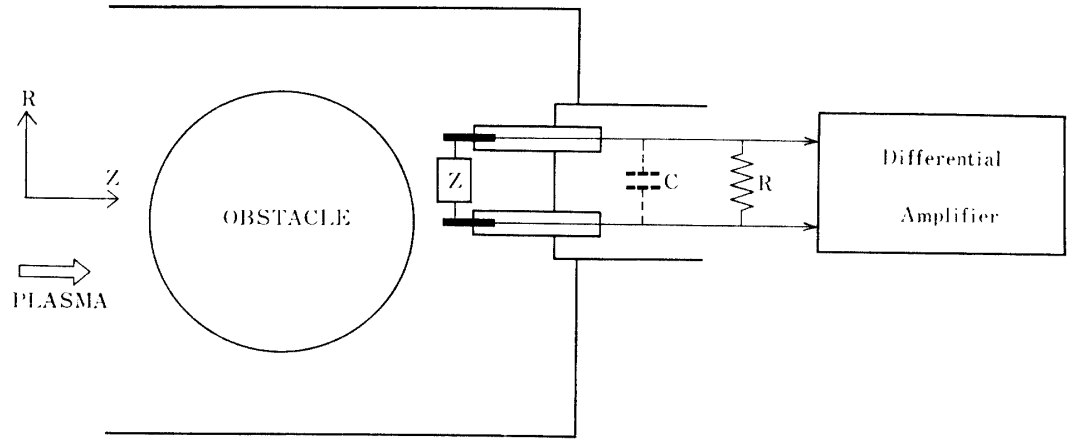

FIG. 2. Method of electric field measurement.

3. RESULTS

The electric field was measured when there were three types of obstacles, namely, aluminum, insulator and gas cloud. The double probe was placed 4 cm behind the center of the obstacle.

Fig. 3(a) shows the double probe and the magnetic probe signal when there is no obstacle. This magnetic probe signal is induced by the diamagnetic current in the plasma. Fig. 3(b) shows the double probe and the magnetic probe signals when there is an insulator sphere. This magnetic probe signal has the opposite sense to the diamagnetic signal of Fig. 3(a), and appears simultaneously with the double probe signal. This double probe signal shows the arrival of main part of the plasma and appears about 40 μsec after the firing of the plasma gun. Fig. 4(a) shows the electric field and the magnetic field signal when there is no obstacle, and shows that the electric field is almost zero. Fig. 4(b) shows the electric field and the magnetic field signals when there is an obstacle, and shows that the electric field signal appears earlier than the magnetic field signal, that is to say, before the main part of the plasma stream comes to the interaction region, and that the electric field disappears when the main part of the plasma enters the interaction region.

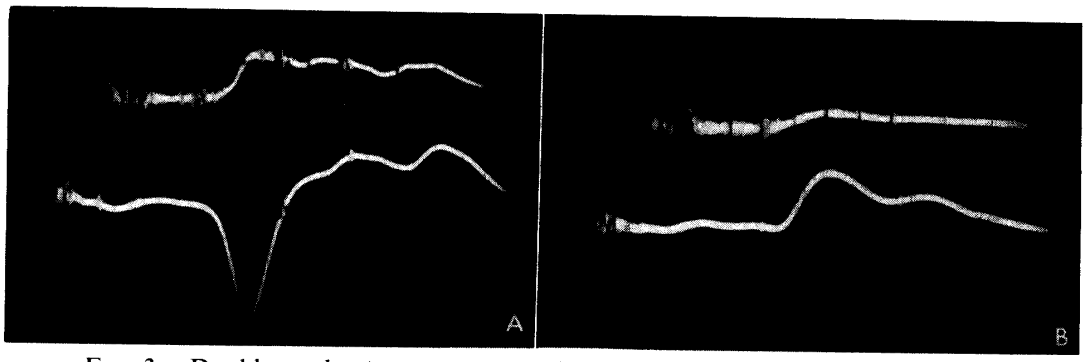

FIG. 3. Double probe (upper trace) and magnetic probe (lower trace) signal. (a): without obstacle (b): with obstacle, Sweep: 10 μs/div.

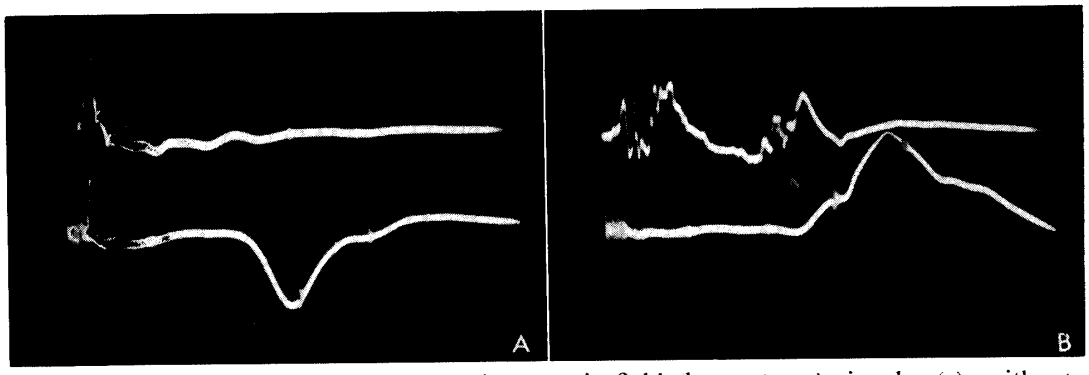

FIG. 4. Electric field (upper trace) and magnetic field (lower trace) signal. (a): without obstacle (b): with obstacle. Sweep: 10 μs/div. Vertical: upper trace 100V/m/div. lower trace 7 gauss/div.

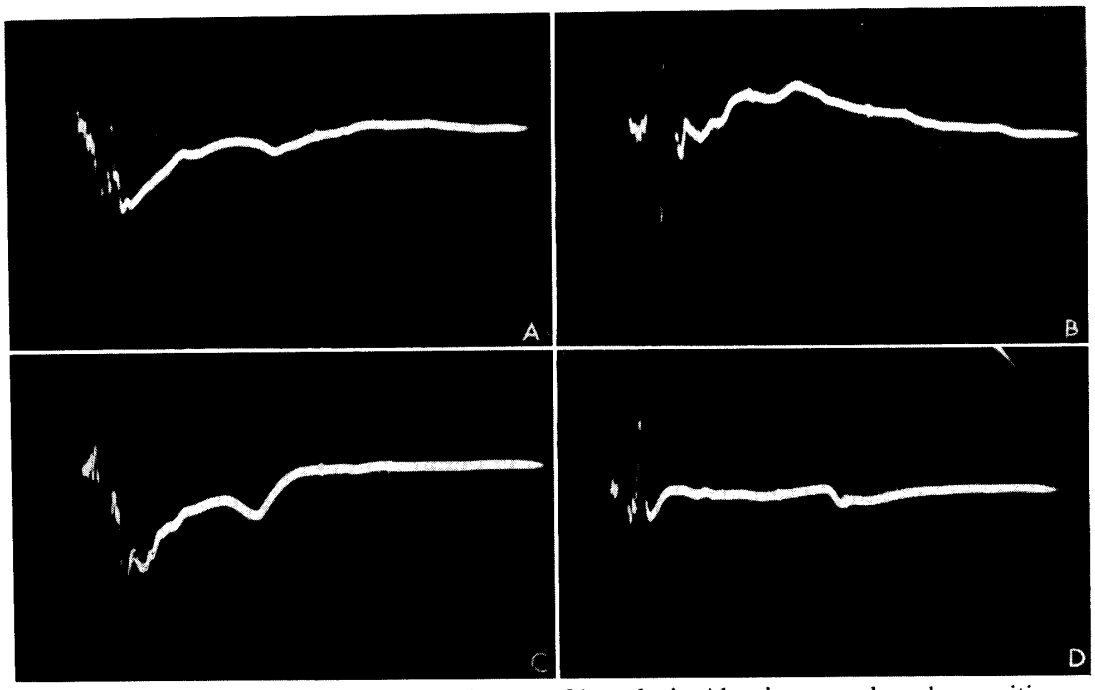

FIG. 5. Typical electric field signals. (a) Obstacle is Aluminum and probe position is +3 cm, (b) Obstacle is Aluminum and probe position is −3 cm. (c) Obstacle is an insultaor and probe position is +2 cm. (d) Obstacle is an air cloud and probe position is +1 cm. Sweep: 10 μs/div.

Figs. 5(a), 5(b), 5(c) and 5(d) show the typical electric field signals when there is an obstacle. $E_r(r)$ is shown in Fig. 6 showing that there is no difference concerning the electric field behind the obstacle whether it is a conductor or an insulator. When the obstacle is a gas cloud, simulating the atmosphere of the planet like Venus, the electric field is almost zero.

4. DISCUSSIONS

Experimental evidence shown in the previous section is explained as follows. Assuming $T_i = T_e$, the gyro-radius of ions and electrons are $r_{gi} = 4$ cm and $r_{ge} = 0.9$

mm, respectively, under the B_{z0} of 95 gauss. Therefore, electrons cannot enter the downstream region of the obstacle, but ions can enter this region since r_{gi} is large compared to the radius of the obstacle. Then, the positive ion rich region appears at the shadow region of the obstacle and the electric field is generated by this charge separation.

This charge separation is diminished by the transverse diffusion of electrons. Diffusion across the magnetic field in a infinite plasma such as space plasma is ambipolar and the effective diffusion coefficient is given by $D_{\perp}^{\text{infinite}} \cong \frac{2}{3} \frac{v_{eth}^2}{\omega_{ce}^2 \tau_{ei}}$, but when the plasma is bounded by a conductor as in this experiment, electrons move along the magnetic field and short circuit the space-charge field there, and the effective diffusion coefficient across the magnetic field is that of ions, namely, $D_{\perp}^{\text{finite}} \cong \frac{1}{3} \frac{v_{ith}^2}{\omega_{ci}^2 \tau_{ei}}$ (Simon [9]).

The characteristic time τ for electrons to diffuse into the gun axis is given by $\tau = \frac{r_0^2}{D_{\perp}^{\text{finite}}}$ where r_0 is the radius of the obstacle. Criterion for the electric field to be generated is that τ is larger that τ_{ci} where τ_{ci} is ion cyclotron period.

Substituting the numerical values of the main part of the plasma stream in this experiment, τ becomes about 4×10^{-2} μsec, while τ_{ci} is 1 μsec. This shows that the charge separation field behind the obstacle is almost zero by the transverse diffusion of electrons.

The gun-produced plasma stream contains the faster component which has a much lower density and a higher temperature than the main part of the plasma stream. The plasma parameters of this faster component are not measured, but assuming $n_p \sim 10^{11}/\text{cm}^3$, and $T_i \sim 16$ eV, τ becomes about 4.8 μsec, satisfying the condition for the electric field to be generated. This electric field is seen in Fig. 4(b). When the obstacle is a gas cloud, the faster component of the plasma stream ionizes this gas cloud and the plasma density in the interaction region increases, resulting in the increase of $D_{\perp}^{\text{finite}}$ and short circuiting of the electric field.

In the actual solar wind at the moon, the characteristic time for diffusion is defined by $\tau_m = \frac{r_{gi}^2}{D_{\perp}^{\text{infinite}}}$ in which r_{gi} is taken for the characteristic length instead of the lunar radius r_l, since r_{gi} is much smaller than r_l and the region where the charge separation should occur is restricted within r_{gi}. This τ_m is much larger than τ_{ci}, so the charge separation electric field would be generated in the boundary region. Though the solar wind is always supplied with the flow velocity V in this case, the electric field would exist downstream the moon, since the diffusion velocity $V_{\perp}^{d} = \frac{D_{\perp}^{\text{infinite}}}{r_{gi}}$ is much smaller than V.

Ness et al. (1968) discussed the perturbation of the magnetic field near the moon, and neglected the effect of the induced electric fields on the magnetic field, but they did not measured and did not discussed the electric field itself.

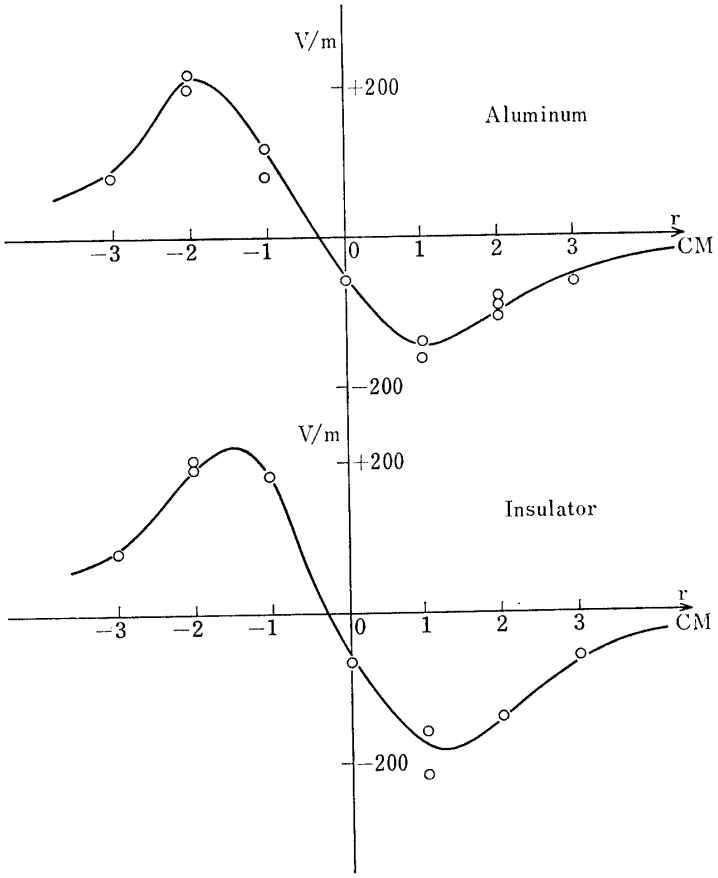

FIG. 6. Spatial distribution of electric field: $E_r(r)$.

In this experiment $r_{gi} \sim 2r_0$, and in practice, the planet that satisfies this condition would be a small planet. For the moon, $r_{gi} \sim 80$ km, and this is much smaller than the lunar radius $r_l \sim 1738$ km.

To simulate the situation on the moon, the external magnetic filed is increased to 1600 gauss ($r_{gi} \sim 2.5$ mm, $r_{ge} \sim 0.06$ mm), and a double probe, with a spacing of 2 mm, is used. The electric field generated in this case is shown in Fig. 7. As seen from Fig. 7, the maximum electric field behind the obstacle was as high as 25 kV/m. Then we can estimate the electric field behind the moon in the downstream of the solar wind from the similarity law.

As the electric field is generated by charge separation in these cases, the simularity law might be based on Poisson's equation, $divE = ne/\varepsilon_0$.

The scaling is as follows: E is scaled as $E_{lab} \rightarrow K_1 K_n E_{\text{space}}$ where the characteristic length and density are scaled as $L_{lab} \rightarrow K_l L_{\text{space}}$ and $n_{lab} \rightarrow K_n n_{\text{space}}$, and $K_l \sim 10^{-8}$, and $K_n \sim 5 \times 10^{13}$, assuming $n_{\text{space}} \sim 2/\text{cm}^3$ and $n_{lab} \sim 10^{14}/\text{cm}^3$, as the magnetic field is 1600 gauss, and $E_{\text{space}} = 5 \times 10^{-2} V/\text{m}$ is obtained.

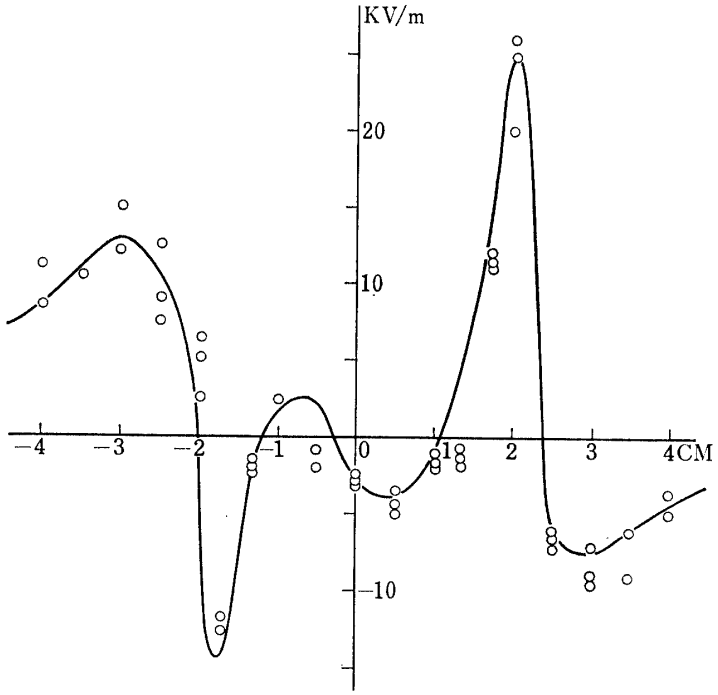

FIG. 7. Spatial pistribution of electric field when the applied magnetic field is 1600 gauss.

In the actual solar wind interaction with the moon, the solar wind contains magnetic field whose direction is not always parallel to that of the plasma flow, so $E_{\text{space}} \sim 10^{-2} V/m$ obtained from the laboratory expetiment under an assumption of the parallelism between the magnetic field and the plasma flow, would not give the electric field in space directly, but gives an upper limit of the electric field generated in space.

For a planet like Venus which is surrounded by a gas cloud, the generated electric field would be short circuited, and no electric field would be observed.

The magnetic field signal is explained as follows: The equation of motion for ions and electrons are given by

$$m_i n_i \frac{d\vec{V}_i}{dt} = en_i\vec{E} - \nabla P_i + en_i\vec{V}_i \times \vec{B}_{z0} \qquad \text{for ions} \qquad (1)$$

and

$$m_e n_e \frac{d\vec{V}_e}{dt} = -en_e\vec{E} - \nabla P_e - en_e\vec{V}_e \times \vec{B}_{z0} \qquad \text{for electrons} \qquad (2)$$

Assuming a stationary state, and a zero electric field when the main part of the plasma stream comes, $V_{i\theta}$ and $V_{e\theta}$ are given by

$$V_{i\theta} = \frac{\partial P_i/\partial r}{en_i B_{z0}} \quad \text{and} \quad V_{e\theta} = \frac{-\partial P_e/\partial r}{en_e B_{z0}}.$$

Ions and electrons drift in opposite directions because of the pressure gradient, and the drift current density is given by

$$j_\theta = en(V_{i\theta} - V_{e\theta}) = \frac{2(\partial P/\partial r)}{B_{z0}} = \frac{2kT(\partial n/\partial r)}{B_{z0}} \qquad (3)$$

Here, $n_i \cong n_e \cong n$ and $P_i = nkT_i = P_e = nkT_e = P$ are assumed.

The plasma density gradient was measured with and without an obstacle. When there is no obstacle, $\partial n/\partial r \cong 0$, and when there is an obstacle $\partial n/\partial r > 0$ as shown in Fig. 8.

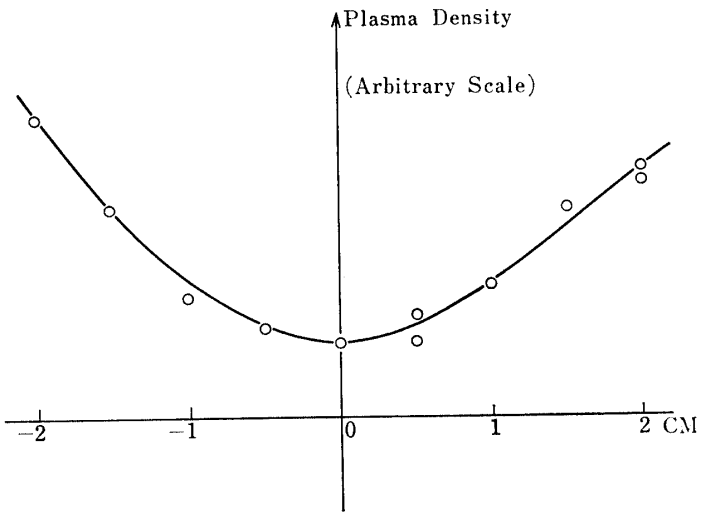

FIG. 8. Spatial distribution of plasma density behind the obstacle.

Therefore, behind the obstacle drift current flows and gives rise to the magnetic field opposite to the diamagnetic signal. No drift current signal appears when there is no obstacle.

Such a magnetic field signal was also measured by Kristoferson, and in the actual solar wind detected by the Explorer 35.

In space, the particle shadowing effects of the moon were observed and the magnetotail electric field was estimated by the data when the moon was in the magnetotail, but the electric field due to the particle shadowing effect itself has not been detected in space, but such a field is likely to exist.

Fig. 9 shows the change in electric field behind the obstacle when the external magnetic field was varied, and shows the electric field oscillation. This would probably be due to the drift instability.

From this it is inferred that the charge separation electric field would be established in the magnetotail of the earth (as $r_{gi} > r_{ge}$) and its oscillation would cause a faster diffusion of the charged particles. Further investigation of this oscillation is now underway by the use of continuous flow of Cs plasma.

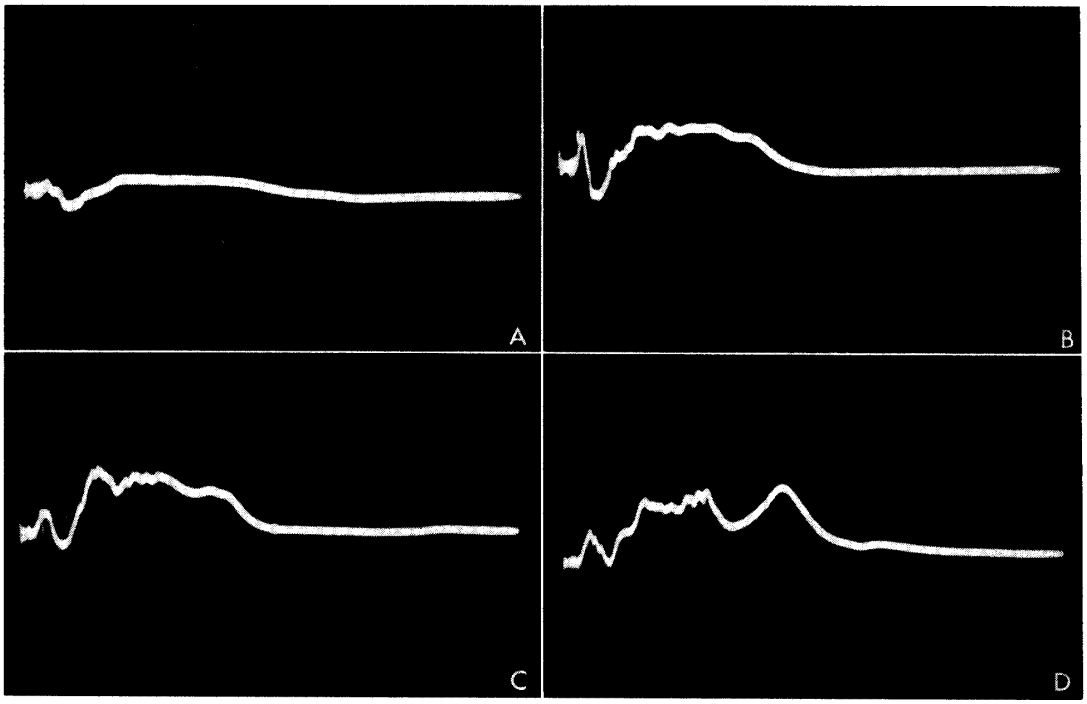

FIG. 9. Electric field and its oscillation when the magnetic field is varied. (a) $B_{z0}=48$ gauss (b) $B_{z0}=95$ gauss (c) $B_{z0}=143$ gauss (d) $B_{z0}=190$ gauss Sweep; 10 μs/div.

5. CONCLUSIONS

There would be an electric field due to particle shadowing effect behind the planets like the moon, and small planets by their interaction with the solar wind. According to the similarity law, the electric field behind the moon is estimated to be in the order of 10^{-2} V/m.

Behind the planets like Venus no electric field would be observed because the surrounding gas cloud short circuits the electric field. This is suggested by the experiment for interaction of the plasma stream with the gas cloud.

The magnetic field measured in this experiment as well as by Kristoferson seems to correspond to the actually observed field by Explorer 35, and the generating mechanism of the magnetic field can be explained by the pressure gradient drift.

ACKNOWLEDGEMENT

The authors wish to thank Dr. N. Kawashima of their Institute for his valuable suggestions and discussions. The authors are also grateful to Prof. N. Fukushima of University of Tokyo for the critical reading of the manuscript.

Department of Space Science
Institute of Space and Aeronautical Science
University of Tokyo, Tokyo
October 28, 1970

[1] Ness, N. F., K. W. Behannon, C. S. Scearce and S. C. Cantarano, Early results from the magnetic field experiment on lunar Explorer 35, J. Geophys. Res., **72**, 5769–5778 (1967)
[2] Ness, N. F., K. W. Behannon, H. E. Taylor and Y. C. Whang, Perturbations of the interplanetary magnetic field by the lunar wake, J. Geophys. Res. **73**, 3421–3440 (1968)
[3] Ness, N. F., The electrical conductivity and internal temperature of the moon, NASA-GSFC preprint X-616-69-191, (1969)
[4] Kristoferson, L., Laboratory simulation experiment on solar wind interaction with the moon. J. Geophys. Res., **74**, 906–908 (1969).
[5] Van Allen, J. A. and N. F. Ness, Particle shadowing by the moon, J. Geophys. Res., **74**, 71–93 (1969)
[6] Anderson, K. A., Method to determine sense and magnitude of electric field from lunar particle shadows, J. Geophys. Res., **75**, 2591–2594 (1970).
[7] Kubo, H., N. Kawashima and T. Itoh, Simulation experiment on the tail of type-1 comets. J. Geophys. Res., **75**, 1937–1939 (1970)
[8] Kubo, H, N. Kawashima and T. Itoh, Interaction of plasma streams with a neutral gas cloud, to be published in Plasma Physics.
[9] Simon, A., Ambipolar diffusion in a magnetic field, Phys. Rev., **98**, 317–318 (1955)